

Ultrafast laser patterning of OLEDs on flexible substrate for solid-state lighting

Dimitris KARNAKIS*, Andrew KEARSLEY and Martyn KNOWLES

Oxford Lasers Ltd, Unit 8 Moorbrook Park, Didcot, Oxfordshire OX11 7HP, UK
 E-mail: dimitris.karnakis@oxfordlasers.com

Rapid developments in the organic LED technology on flexible foils promise to deliver thin, lightweight and power-efficient light sources for intelligent lighting applications. Laser patterning of OLEDs on glass for display applications has been widely reported. However, fewer reports discuss patterning of OLEDs on flexible substrates, which presents a novel optical engineering challenge. Our aim here is to quantify the potential of picosecond lasers for this application and determine a robust laser process window for large area selective OLED electrode patterning. This should involve the complete removal of (i) 130 nm thick ITO anode on a barrier layer stack and (ii) 100 nm thick Ba/Al cathode on 180 nm thick LEP/PEDOT:PSS active organic layers while leaving intact all underlying layers. Detailed laser ablation studies at 532 and 355 nm reveal that ps lasers uniquely facilitate roll-to-roll OLED manufacturing by providing fine resolution. Damage thresholds, process quality and process speed limitations will be discussed. Careful crater examination reveals that the choice of laser pulse duration is more important than wavelength for a given layer thickness. A photomechanical stress-induced ablation mechanism is believed to be key for this process and debris-free, low temperature patterning can be achieved.

Keywords: OLED, ITO, thin-film patterning, picosecond laser ablation, stress-assisted ablation

1. Introduction

Rapid developments in OLED technology are beginning to make significant inroads to the commercial world [1] with OLED displays already available in certain niche applications. Lasers are typically used in OLED manufacturing for patterning the active layers or the transparent oxide and metal thin-film electrodes [2,3]. Research has even shown that lasers can be used to deposit OLED layers on demand via a direct-write dry printing method called laser-induced forward transfer (LIFT) [4].

Commercial interest is now growing in producing large area OLEDs on plastic foils for intelligent solid-state lighting [5]. These roll-to-roll manufactured foils promise to deliver thin, lightweight and power-efficient light sources for general, architectural or automotive lighting and signage applications. However, most flexible plastic substrates are permeable to water and oxygen and cannot provide adequate OLED encapsulation. To avoid severe device degradation, a transparent thin-film stack of several organic/inorganic barrier layers must be incorporated between the OLED films and the plastic substrate (Figure 1) [6]. Manufacturing these barrier layers represents a great challenge. Selective laser patterning therefore of the thermally thin OLED films atop such barrier layers is even more demanding, as any laser structuring must leave them totally unharmed. Additionally any contamination from laser-generated debris is severely prohibited to avoid long-term degradation of the OLED device performance and lifetime.

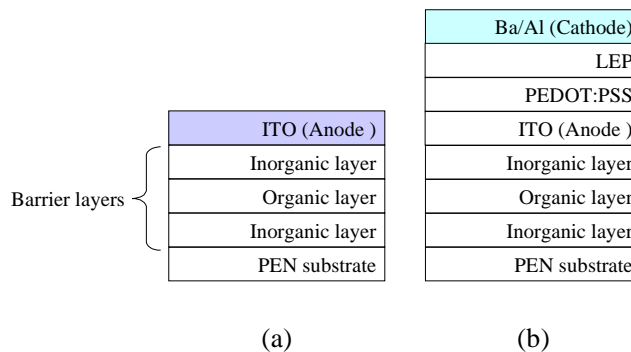


Fig. 1 Multilayer OLED stack on PEN substrate. Laser patterning of (a) the anode layer on a barrier stack and (b) the cathode layer on the light-emitting layer (LEP) is necessary.

In other words, laser ablation must proceed via a low temperature removal mechanism suppressing any thermal characteristics that could potentially damage the OLED or its multilayered substrate. This is preferably accomplished using ultrafast lasers via a stress-assisted film fracture and ejection (spallation) ablation mechanism rather than involving vaporization or other phase change.

Our aim [5] is to quantify the potential of picosecond lasers for patterning a 130 nm thick ITO film on the barrier layer and a 100 nm thick cathode bilayer (Ba/Al) on the organic light emitting layer (LEP) and ideally determine a process window for large area selective OLED patterning.

2. Selective laser patterning of OLEDs by stress-assisted ablation

For stress-assisted ablation to occur both the thermal and stress confinement criteria must be fulfilled in the absorbing layers [7]. This means that (a) maximum light absorption in the film is required with minimum thermal conduction losses away from the irradiated area and (b) rapid heating to produce very high transient thermoelastic stress to exceed the film fracture limit before any thermal expansion allows for stress relaxation. Therefore both laser wavelength and pulse duration seem critical.

The characteristic times to consider further are: (i) the thermal relaxation time τ_{th} i.e. the time needed to dissipate heat generated by the laser pulse, given by $\tau_{th} = \delta^2/4\chi$ and (ii) the acoustic relaxation time τ_{ac} , i.e. the time needed to initiate a collective motion of atoms or molecules within the absorbing volume, given by $\tau_{ac} = \delta/C_s$. Here δ refers to the smallest dimension of the heated volume, typically the laser or thermal penetration depth assuming a much larger laser spot size, χ is the film thermal diffusivity and C_s is the sound speed in the film.

If the laser pulse duration τ is shorter than the thermal relaxation time τ_{th} ($\tau < \tau_{th}$), the thermal confinement criterion is fulfilled maximising the temperature in the heated volume by restricting thermal diffusion to the substrate layers and efficiently generating thermoelastic stress. Additionally, if the laser pulse duration is shorter or comparable to the characteristic acoustic relaxation time τ_{ac} ($\tau < \tau_{ac}$), laser heating of the target will proceed at nearly constant volume. The heated material will have little time to expand and the large temperature gradients will cause a buildup of high compressive stresses. The interaction of the laser-induced compressive stresses with the free surface of the irradiated sample can then result in generation of tensile stresses, sufficiently high, that can overcome the dynamic strength of the material causing mechanical fracture or promote cavitation and fragmentation in a metastable liquid [8]. With this approach differences in thermal expansion between the stack layers can be neglected as the strain is assumed negligible.

Since ITO absorbs weakly at 355 nm with a laser penetration depth of $\sim 2.4 \mu\text{m}$ ($\alpha_{355} = 4100 \text{ cm}^{-1}$), uniform film heating is assumed through the entire film along the beam propagation. Taking $\delta = 130 \text{ nm}$, results in thermal and acoustic relaxation times of 2 ns and 43 ps respectively as shown in Table 1. This means that a laser pulse shorter than $\sim 43 \text{ ps}$, will satisfy both the thermal and stress confinement criteria for stress-assisted ablation of ITO restricting thermal diffusion to the barrier layers and

efficiently generating thermoelastic stress in the film. However, as only a small fraction of the incident energy will be deposited in the weakly absorbing ITO, care should be taken to avoid optical damage from direct absorption in the underlying barrier layers by keeping the incident intensity low below the barrier ablation threshold.

The metal cathode bilayer (Ba/Al) absorbs strongly at UV, visible or IR wavelengths and hence irradiation at 532 nm ($\alpha_{532} = 1.2 \times 10^6 \text{ cm}^{-1}$) is expected to remove the cathode layer while leaving unharmed the transparent LEP layer underneath. The laser heated volume estimation is key for determining the thermal and acoustic relaxation times here. The optical penetration depth is very short at 8.3 nm and laser heating of the film will thus be dictated by thermal diffusion during the laser pulse. Since the thermal response of metals to ultrafast excitation is a non-equilibrium process with different electron and lattice heating rates, the classical square root dependence of heat diffusion on laser pulse duration does not apply. Our estimate of the thermal diffusion depth based on [9] is 72 nm using an electron-phonon coupling constant for Al of $3.1 \times 10^{17} \text{ W/m}^3\text{K}$ [10] and a weaker dependence on laser pulse duration $\tau^{0.2}$. With $\delta = 72 \text{ nm}$ for a 10 ps laser pulse, both thermal and acoustic relaxation times are approximately equal at $\tau_{th} \approx \tau_{ac} = 13 \text{ ps}$.

3. Experimental

Both laser sources used here are commercially available DPSS mode-locked Nd:YVO₄ amplifiers emitting laser pulses of 10 ps (FWHM) duration. For ITO patterning an Oxford Lasers Picolase 1000 micromachining system was used at 355 nm. The laser repetition rate was fixed at 10 kHz and the beam was focused with an f-theta telecentric lens ($f = 100 \text{ mm}$) to an estimated spot size of $32 \mu\text{m} \varnothing$. The focussed spot was translated across the ITO surface using a galvanometer scanner with maximum translation speed of 2 m/s. The sample consisted of a 130 nm thick ITO layer sputtered on a multilayered barrier stack of PECVD deposited SiN / organic planarisation layer / SiN layers having thicknesses of 300nm / 40 μm / 300nm respectively. These were deposited on a 100 μm thick PEN foil. All layers underneath the ITO were transparent between 400-800 nm. The SiN absorption coefficient at 355 nm is estimated as $\alpha = 1.35 \times 10^4 \text{ cm}^{-1}$.

For cathode patterning a Coherent Talisker 532-8 was used at 532 nm. A similar beam delivery setup was utilised to focus the beam to a 35 μm diameter spot. Single or multiple pulse ablation tests were conducted by controlling the incident number of laser pulses per area. The cathode sample consisted of a metal bilayer (thickness: Al 100 nm, Ba 5 nm) thermally evaporated on the OLED layers (80 nm thick white emitting LEP and 100 nm thick conductive Poly 3,4-ethylenedioxythiophene polystyrenesulfonate (PEDOT: PSS)). The OLED layers were slot-die coated on the ITO anode. All layers underneath the cathode were transparent at 532 nm.

Ablation took place in air and the etched layers were vacuum extracted above the target. In both cases, the pulse energy was varied using a half-waveplate and polarizer attenuation setup. The ablated samples were investigated with an optical microscope or white light interferometer.

Table 1 Estimated thermal and acoustic relaxation times for 10 ps laser irradiated OLED thin-film electrodes

Material/ thickness	δ (nm)	χ (cm ² /sec)	C_s (m/s)	τ_{th} (ps)	τ_{ac} (ps)
Anode (130nm)	130	0.0216	3045	1950	43
Cathode (100nm)	72	0.9986	5300	13	13

4. Results and discussion

4.1 Laser patterning of ITO on barrier layers

By varying the input pulse energy and scanner speed, a range of incident laser fluences at different pulse overlaps were examined for ITO line scribing. The average fluence ablation threshold at 355 nm for single-pulse ablation was determined as 50-55 mJ/cm². Below this value no ablation was recorded. At fluences between 75-130 mJ/cm² ITO ablation was also accompanied by surface roughening of the underlying SiN barrier layer.

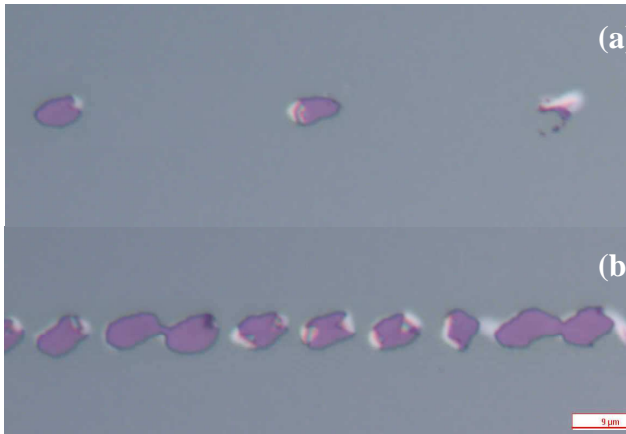


Fig. 2 High magnification (500x) optical images of 10ps laser scribed ITO (grey) on barrier stack (purple) for OLED fabrication. (355 nm, 62 mJ/cm²) (a) one pulse (300 mm/s) and (b) four pulses per area (75mm/s). The ablated craters are a fraction of the illuminating laser spot on target. Bar denotes 9µm

Figure 2 shows scribed lines in ITO at 62 mJ/cm² just above threshold, using one (fig.2a) or four (fig.2b) overlapping pulses per area. Non-continuous lines of discrete irregular shaped craters were obtained in both cases, seemingly elongated in the direction of scanning. This implies that the ablation threshold was only exceeded locally by a very narrow intensity part near the tip of the focused Gaussian beam. The ablated films appear to have been removed intact with no damage to the underlying SiN. There is also no evidence for melting or any other phase-change and by and large, no debris was found scattered in or around the craters, suggesting that ITO and the barrier layers have probably experienced very low temperature rise.

The fractured morphology of the craters reveals clearly the photomechanical character of ablation in this case. This is particularly evident near the crater edges where partially ablated ITO was found as lifted off flakes, which were still attached to the parent film and clearly not thermally decomposed. In some cases also, very few unsuccessfully extracted ablated layers, were located nearby the craters as softened curled up flakes, supporting this view further.

By adjusting the scribing speed the ablated craters can be joined to form an uninterrupted continuous scribed line on ITO. Depth profile measurements of the scribed line (Fig.3) confirm clean ablation with smooth uniform floors,

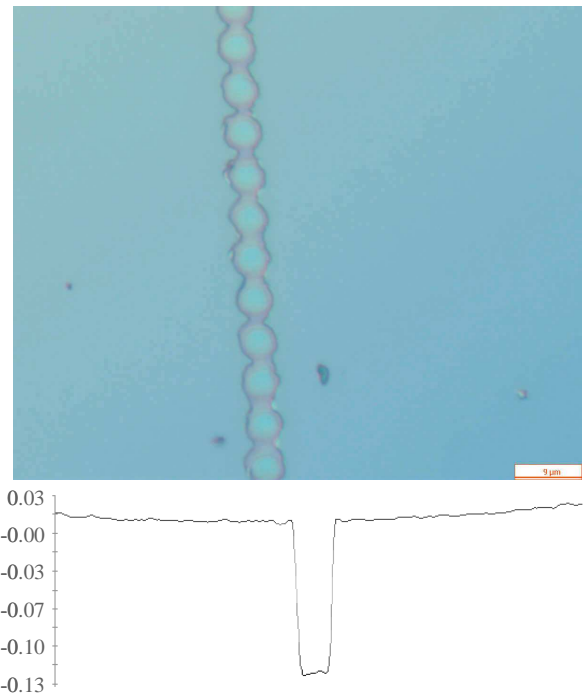


Fig. 3 Optical image of scribed line in ITO using a 355nm 10ps focused Gaussian beam. Optical profiler depth measurement of 355nm, 10ps ablated ITO crater; scribed depth: 123nm, crater width: 9-12µm, (Y) scale: 15nm/div

no raised edges in the adjacent unexposed areas and an etched depth of 123 nm indicating that only ITO has been removed from the stack. Furthermore, electrical continuity measurements confirmed that such lines could be used to create electrically isolated OLED tiles.

Very similar ablation results, not reported here, have been preliminary achieved with IR (1064 nm) and visible (532 nm) picosecond lasers ($\tau=10ps$) incident, either directly on the ITO surface or through the transparent foil, suggesting that ITO patterning on a barrier stack shows limited wavelength dependence.

Although the adhesion strength between films in the current stack was not measured, overcoming ITO adhesion to the barrier layer is expected to be undemanding in the order of few tens of $\mu J/cm^2$ [11]. In photomechanical ablation, small fractions of the absorbed laser energy go into overcoming film adhesion to the substrate and mostly go into elastic stress energy. A portion thereof is used into plastic deformation of the target, generation of internal free surfaces (fracture by generation of cracks or voids), and kinetic energy of the ejected material. Negligible energy goes into a phase change, except some evaporation into voids and cracks [7]. This is in contrast to fracture due to an explosive phase change when the driving force is the pressure in expanding vapor bubbles.

That agrees well with the experimental findings here and is in line with energy balance considerations. The input energy load $E_L = (1-R)\alpha F_p$ at threshold in ITO is estimated as 436 J/cm³ using a thin-film stack reflectivity $R = 3.2\%$ at 355 nm, $\alpha = 4100 cm^{-1}$ and peak fluence $F_p = 0.11 J/cm^2$. Neglecting any heat losses and with an input load much lower than the melting or vaporisation enthalpies, all absorbed energy will be used to raise the film temperature

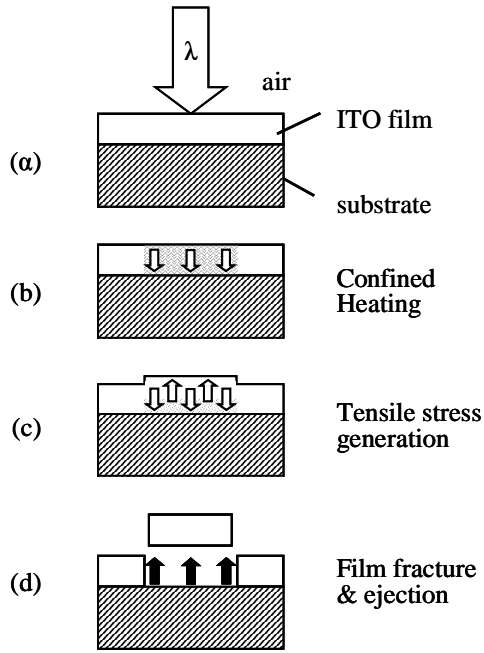


Fig. 4 Schematic representation of stress-assisted ITO film ablation on barrier substrate layer; (a) $t=0$, light absorption, (b) rapid laser heating under thermal and stress confinement, maximum compressive thermoelastic stress (c) thermal expansion relaxation with tensile stress generation, (d) tensile strength exceeded, film fracture and ejection

by $\Delta T = E_L/\rho C$. With ITO density $\rho = 7.1 \text{ g/cm}^3$ and specific heat $C = 340 \text{ J/kgK}$, this is estimated as only $\Delta T = 181\text{K}$, well below the melting point of 2100 K . Since ITO is weakly absorbing at 355 nm , it is reasonable to assume the film is uniformly heated across its entire thickness along the beam propagation. The maximum uniaxial thermoelastic compressive stress $\sigma = \alpha E \Delta T$ generated in the film under stress confinement (no strain during heating) can then be estimated as 150 MPa with linear thermal expansion coefficient $\alpha = 7 \times 10^{-6} \text{ K}^{-1}$ and Young's modulus $E = 118 \text{ GPa}$. Although a definite ablation route is not entirely clear in the absence of more experimental information, it is feasible that a large enough tensile stress component can subsequently develop in the film upon relaxation, which can exceed the ITO tensile strength and cause film fracture and ejection. Reported values for ITO tensile strength of 125 MPa [12] could support this notion.

The role of the substrate cannot be ignored [13] due to the weak ITO absorption, as the SiN layer will absorb part of the transmitted energy. No ablation of the SiN takes place though below 75 mJ/cm^2 . Although difficult to approximate the exact input load on that film due to thin-film interference [14], a significant temperature rise estimated as $\sim 2300 \text{ K}$ could be present at the ITO-SiN interface which is probably approaching the current SiN film melting point. For the present film stack, values of $R(\text{SiN}) = 26.6\%$, $\alpha = 1.35 \times 10^{-4} \text{ cm}^{-1}$ and a peak fluence of 0.1 J/cm^2 were used. Such high temperature would certainly cause transient interface displacement and although the thermal expansion of the current SiN layer matches well that of ITO, it cannot be excluded from partly

contributing to the overlying ITO ablation. The possibility of expanding vapour originating at the SiN surface to blow off the ITO layer cannot be excluded, although no visible surface changes were detected on the barrier layer below 75 mJ/cm^2 . Also, as mentioned above, very similar ITO ablation results were recorded with laser irradiation at 532nm and 1064nm where the SiN is totally transparent. Further experimental evidence investigating this effect microscopically is necessary to clarify the process.

Essentially, since ablation is based on single-pulse removal, process speed limitations are likely to arise from the maximum available laser output and the ability to separate the delivered laser pulses at the workpiece at high repetition rates with an appropriate beam delivery and motion control setup. Also the stress profile in the film is directly related to the gradient of the incident laser intensity profile. Sharper gradients at the spot edges from a reshaped Gaussian beam are expected to provide cleaner boundaries with less delamination. Ca tests are currently in progress to examine the barrier layer integrity from picosecond laser ablation of ITO before proceeding further.

4.2 Laser patterning of Ba/Al cathode on light emitting polymer (LEP)

Single-pulse ablation of the Ba/Al cathode bilayer on active OLED layers was investigated using picosecond 532 nm laser irradiation. The aim was to cleanly remove the cathode while leaving intact all underlayers. Since an 80 nm thick white light emitting polymer (LEP) layer was in direct contact below the cathode, a visible wavelength (532 nm) was chosen where both organic layers (LEP and PEDOT:PSS) as well as the ITO and barrier layers show negligible absorption, in contrast to the cathode. The cathode reflectivity is almost constant between $500\text{-}1000 \text{ nm}$.

A series of single-pulse ablated craters with increasing pulse energy E_p on target was measured. Both the crater diameter and depth increased with E_p , as expected, due to the almost Gaussian intensity profile of the focussed spot. By plotting therefore the measured crater squared diameter against the pulse energy (Fig.5), a single-pulse ablation threshold for cathode removal was estimated as 95 ± 9

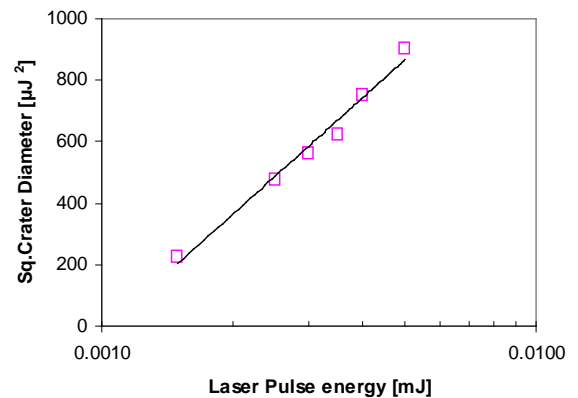


Fig. 5 Ablated crater area v incident laser pulse energy for 532nm , 10ps single pulse ablation of Ba/Al cathode on OLED layers. The fitted curve slope reveals an ablation threshold of $95 \pm 9 \text{ mJ/cm}^2$

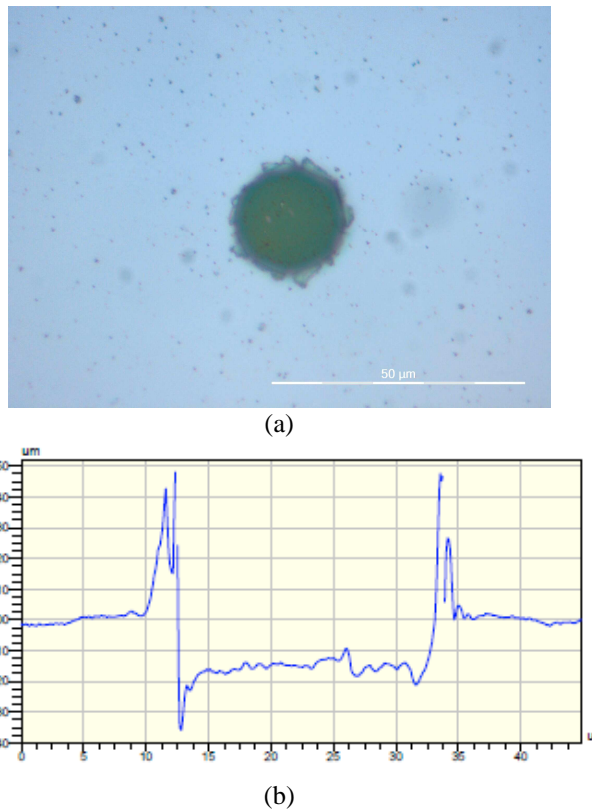


Fig. 6 (a) Optical microscope image of ps laser ablated cathode crater on LEP. Single pulse ablation, 532nm, 10ps, 2.5μJ; Bar 50μm. (b) Depth profile of the ablated crater, depth~140nm. Scale (X):2.5μm/div, (Y):25nm/div.

mJ/cm² from the slope of the fitted curve.

Laser irradiation at fluences between 137-360 mJ/cm² removed the cathode layer only, resulting in a uniform flat floor and an intact LEP surface, allowing a relatively wide process window for cathode removal. A typical example of such laser patterned Ba/Al cathode layer on the OLED stack is shown in figure 6. The average fluence was 230 mJ/cm² irradiated with an estimated spot diameter at 1/e² of 35 μm. This resulted in a crater diameter of 21.5 μm. One drawback with the current optical setup is the relatively rough crater boundaries obtained during rupturing from the non-uniform spatial irradiation. These irregular shaped edges are typically folded back towards the adjacent unirradiated surface, contributing to a rim elevation of 500 nm or more, which can be detrimental to further processing steps. Introducing a more uniform beam profile, comparing to the present Gaussian beam, might reduce this effect. Interestingly, there is hardly any newly introduced laser-induced microdroplets or other “thermal signature” debris redeposited around the crater. That is good evidence of a low temperature removal process and quite encouraging for OLED manufacturing as the presence of surface microparticles is linked to the introduction of black spots and faster degradation of the OLED device performance and lifetime.

At higher fluences ($F > 360$ mJ/cm²), two or more layers were ablated simultaneously and the craters were deeper at the centre, due to the higher Gaussian intensity locally. Similarly, multiple pulse irradiation created deeper craters

by removing the underlying organic layers also. In both cases the stepped ablation craters point to the deterministic character of the removal process. The craters remained sharp with clean edges even at the highest examined fluence of 825 mJ/cm².

Laser removal of metal films on polymer substrates is generally considered challenging, metal ablation being energetically more expensive with the potential to easily damage a sensitive underlayer. Unlike nanosecond UV ablation of metals [15] where the ablated films are blown off in a liquid phase via a substrate assisted explosive removal, picosecond laser patterning can permit precise metal removal with little, if any, melting involved and generally limited thermal characteristics depending on the chosen laser parameters [16] and quality of film contact.

An exact mechanism for the clean metal removal in this case still remains unclear. When the laser pulse duration is of the order or shorter than the electron-phonon thermalisation time, laser matter interaction is a two-step, non-equilibrium heating process. The incident laser energy is absorbed by electrons during excitation and soon after a portion is transferred to the lattice through electron-phonon coupling. Meanwhile the hot electrons diffuse deeper in the material extending the heated depth. Both thermal and stress confinement criteria will be satisfied using a 10 ps laser pulse and the metal layer will therefore become highly compressed upon laser heating. At low fluences, a strong shock wave is generated by a hot-electron blast force early on that weakens the material. This is compounded by the thermal load from the subsequent lattice heating after the laser pulse which could generate enough thermoelastic stress to exceed upon relaxation an expected tensile strength for Al of 450 MPa and result in film fracture [17]. Such a qualitative explanation can support the observed lack of cathode melting during low power picosecond laser patterning.

It can also be argued though that diffusing heat from the irradiated cathode can raise the LEP temperature. Assuming a slow “heat leaking” rate from the LEP film to the further underlying PEDOT:PSS film, it is plausible that this temperature rise could cause thermal expansion of the LEP surface or even some degassing of hot escaping products from a non-decomposed LEP film and generate enough pressure behind the metal film that could contribute to the detachment of the anyway softer cathode near the melting point. Permanent damage from swelling observed on the LEP surface upon cathode ablation at slightly higher fluences could point to such an ablation route. Further experimental evidence exploring the timescale of cathode ablation on a multilayered OLED could clarify the removal mechanism further.

5. Summary

Experimental evidence suggests that selective laser patterning of multilayered OLED stacks is enabled using picosecond lasers at visible and UV wavelengths. Transparent ITO anode films on inorganic barrier layers or metal cathode on organic OLED layers can be cleanly removed without damage to the underlying layers most likely by a stress-assisted low temperature ablation process.

Acknowledgments

The authors gratefully acknowledge financial support from EU program FP7 ICT-3 FAST2LIGHT, No: 216641 and IMEC (Ghent, BE), Coherent Scotland, (Glasgow, UK) and Microbridge Services Ltd (Cardiff, UK) for access to their lasers, metrology equipment and helpful discussions with Piet Bouten, Philips Research (Eindhoven, NL).

References

- [1] S.R.Forrest, Nature, 428, (2004) 911-918
- [2] D.Lidzey, M.Voight, C.Gibeler, A.Buckley, J.Wright, K.Boehlen, J.Fieret, R.Allott, Org. Electr. 6 (2005) 221
- [3] Y.Ito, Y.Onodera, R.Tanabe, M.Ichihara, H.Kamada, Proc.SPIE 6458 (2007) 64580C.1
- [4] R.Fardel, M.Nagel, F.Nuesch, T. Lippert, A,Wokaun, Appl.Phys.Lett., 91 (2007) 61103
- [5] www.fast2light.org
- [6] J.D.Affinito, M.E.Gross, C.A.Coronado, G.L.Graft, I.,N.Greenwell, P.M.Martin Thin Solid Films 290-291, (1996) 63
- [7] G.Paltauf and P.E.Dyer, Chem.Rev. 103 (2003) 487
- [8] E.Leveugle, D.S.Ivanov, L.V.Zhigilei, Appl. Phys. A 79, (2004) 1643
- [9] P.B.Corkum, F.Brunel, N.Sherman, T.Srinivasan-Rao, Phys.Rev.Lett., 61 (1988) 2886
- [10] Z.Lin, L.V.Zhigilei, V.Celli, Phys.Rev.B 77 (2008) 75133
- [11] S.G.Koulikov and D.D.Dlott, J. Photoch. Photobiol A: Chem 145, (2001) 183
- [12] www.Bizesp.com
- [13] O.Yavas and M.Takai, J.Appl.Phys. 85 (1999), 4207
- [14] D.Bauerle "Laser Processing and Chemistry" (Springer, Berlin 1996) p.128
- [15] P.E.Dyer, D.M.Karnakis, P.H.Key, D.Sands, Appl.Surf.Sci., 109/110 (1997) 168
- [16] J.Yang, Y.Zhao, N.Zhang, Y.Liang, M.Wang, Phys.Rev B., 76 (2007) 165430
- [17] J.K.Chen, J.E.Beraun, C.L.Tham, Int.J.Eng.Sci. 42 (2004) 793